Theoretical Chemistry Accounts (2020) 139:158
https://doi.org/10.1007/s00214-020-02672-2

REGULAR ARTICLE

Theoretical study of the adsorption of amantadine on pristine, Al-, Ga-, P-, and As-doped boron nitride nanosheets: a PBC-DFT, NBO, and QTAIM study

Mohsen Doust Mohammadi[1] · **Hewa Y. Abdullah**[2]

Received: 17 July 2020 / Accepted: 1 September 2020
© Springer-Verlag GmbH Germany, part of Springer Nature 2020

Abstract
Nowadays, nanostructures such as nanotubes and nanosheets are widely used in industry, especially the medical industry, for drug delivery, prevention and treatment. In the present investigation, the feasibility of detecting the amantadine gas molecule onto the outer surface of pristine single layer boron nitride nanosheet, as well as its aluminum (Al)-, gallium (Ga)-, phosphorus (P)-, and arsenic (As)-doped structures, was carefully evaluated. For achieving this goal, a periodic boundary condition density functional theory level of study using the HSEH1PBE functional together with a 6-311G (d) basis set has been used. Subsequently, the B3LYP-D3, wB97XD, and M062X functionals with a 6-311G (d) basis set were also employed to consider the single point energies. Subsequently, the B3LYP-D3 (BJ)/6-31G (d) method was also used to consider the contribution of scattering interactions to energy analyzes, natural bond orbital and quantum theory of atoms in molecules and the results were compatible with the electronic properties. In this regard, the total density of states, the Wiberg bond index, natural charge, natural electron configuration, donor–acceptor natural bond orbital interactions, and the second-order perturbation energies are performed to explore the nature of the intermolecular interactions. All of the calculations and analyses denote that by adsorbing of the amantadine molecule onto the surface of pristine boron nitride nanosheet, the adsorption is of the type of physical adsorption and van der Waals interactions. Among the doped nanotubes, gallium-doped nanotube has a very high adsorption energy compared to other elements, and is expected to be chemically adsorbed in this case and appears to be a suitable drug delivery option.

Keywords Amantadine · Density functional theory · NBO · Atom in molecule · Natural bond orbital

1 Introduction

The nanomaterials are structurally divided into carbon and non-carbon materials. Carbon nanotube (CNT) was first discovered independently by Iijima and Ichihashi in 1991 in soot from carbon discharge in a neon-containing medium [1]. CNTs are able to pass through the cell wall because of their needle shape [2]. Subsequently, for the first time in 1995, boron nitride nanotubes (BNNTs) were synthesized [3, 4]. These BNNTs, like CNTs, have excellent mechanical properties due to the strong sp^3 bonds in the wall of the nanosheet [5, 6]. Boron nitride nanosheet (BNNS) like graphene sheet consists of the juxtaposition of hexagonal rings, honeycomb structure, developed in two dimensions [7]. The method of synthesizing nanosheets of boron nitride, which, unlike graphene, are not suitable conductors for electric current, is described here [8–12]. In summary, these nanoparticles are obtained from the chemical vapor deposition of borazine at very high temperatures.

BNNSs are characterized by remarkable mechanical and electrical properties such as wide band gap (5–6 eV), such a large band gap makes the BNNS act as an electrical insulator [12–14]. Among the nanosheets, the very high thermal conductivity of BNNS is exemplary [15–17]. The physical and chemical properties of layered structures are directly related to the number of layers, so that in the case of graphene, the properties change dramatically with increasing layers [18]. But in the case of boron nitride nanosheets, the properties of

✉ Hewa Y. Abdullah
hewayaseen@gmail.com

[1] School of Chemistry, College of Science, University of Tehran, Tehran 14176, Iran

[2] Physics Education Department, Faculty of Education, Tishk International University, Erbil 44001, Iraq

Published online: 12 September 2020

the single-layer structure are close to those of the multi-layer structures. For instance, high thermal and chemical stability, and high oxidation resistance is not really thickness dependence [19–21]. Due to the presence of such properties, in the industry, many uses of boron nitride nanosheets are widely used. For example, due to the proton transfer property, these materials are used in fuel cells [22]. It can also be used as a valuable material in the coating industry and metal protection, because it is impermeable to gases and liquids and is also an electrical insulator [20, 23–25].

In the last two decades, theoretical studies in the density functional theory (DFT) framework on nanostructures have attracted the attention of many scientists in the fields of computational chemistry and solid-state physics. The study of boron nitride nanosheet is no exception, and many theoretical studies on this nanostructure have led to interesting proposals for the manufacture of industrial devices. Omidirad and Azizi [26] showed that when H_2O molecule placed on the VD-8*8BNNS cavity, it will dissociatively chemisorbed. Esrafili et al. have investigated widely various theoretical researches in order to adsorb different molecules such as NO [27], CO [28], CH_2O [29], $COCl_2$ [30], C_2H_4 [31], and N_2O [32] on the surface of pristine and decorated boron nitride nanosheet. Mohammadi et al. [33] have studied the adsorption of halomethanes onto the BN-, Al-/Ga-doped nanosheets. Rossini et al. [34] showed the characterization of *h*-BNNS molecular edge terminations. In Shao et al. [35] BNNS@Ti_3C_2 was used as an electrocatalyst. Azamat et al. [36] had an interesting simulation for the separation of copper and mercury using BNNS, and many other researches, all of which cannot be mentioned here [37–40]. The widespread use of boron nitride nanosheets provides the basis for further study on such structures.

The amantadine molecule is the basis of many new drugs and chemicals amantadine was first discovered by Davis in 1964 and was used to treat the flu virus [41]. Amantadine is a member of adamantane branch when an amino group joins to one of the four most stable methine positions in adamantane to form $C_{10}H_{17}N$. This molecule is used in antiviral drugs and in the treatment of Parkinson's and influenza A infections [42].

This study discusses about the interactions of amantadine (AMD) with BNNS and BN nanosheets doped with Al, Ga, P, and As, elements. After optimizing the structure of boron nitride nanosheets by Gaussian software, to study the chemical stability and conductivity, the elements doping process on this nanosheet have been studied. Because of the high sensitivity of computation to precisely determine the energy of molecular orbitals to investigate the conductivity and probability of physical and chemical adsorption, different structures need to be optimized using appropriate computational methods. For this purpose, the HSEH1PBE functional and 6-311G (d) basis set was used in this research for computation. The B3LYP-D3, wB97XD, and M062X functionals with 6-311G (d) basis set were also used to calculate the single point energies. Natural bond orbital and quantum theory of atoms in molecules were studied by using the B3LYP-D3/6-311G (d) method and the results were used to obtain various physical parameters.

2 Computational details

The DFT calculations at Heyd–Scuseria–Ernzerhof () functional [43] together with 6-311G (d) Pople split-valence triple-zeta basis set with polarization functions [44] were used for geometry optimization for all different positions of the AMD/sheet complex structures. To determine the stability of the optimized structures, frequency calculations are also performed using the similar level of theory to approve that all the stationary points are in agreement with a minimum point through the potential energy surface. For further investigation, single point energy calculations using different levels of theory were also applied on the most stable relaxed structures, which were obtained from geometry optimization at the HSEH1PBE/6-311G (d) level. The levels of theory used for the single point energy calculations included B3LYP-D3, M06-2X, wB97XD together with 6-311G (d) basis set. Natural bond orbital (NBO) and quantum theory of atoms in molecules (QTAIM) were implemented by using the B3LYP-D3/6-311G (d) method. All of the calculations including geometry optimization, single point energy calculations, and NBO analysis were performed by Gaussian 16 package [45]. It should be noted that the NBO calculations were performed using NBO v 3.0 software which is embedded within Gaussian software. In order to perform quantum theory of atoms in molecule (QTAIM) and density of state (DOS) analyses, the Multiwfn program [46–48] was employed.

The adsorption energy (E_{ads}) of the investigated AMD onto the surface of pristine and doped nanosheets can be calculated as follows:

$$E_{ads} = E_{sheet/AMD} - \left(E_{sheet} + E_{AMD}\right) \quad (1)$$

where $E_{sheet/AMD}$ represents the total energy of the complex structure. E_{sheet} and E_{AMD}, are the total energy of the pure nanosheet and the pure AMD molecule, respectively. It is noteworthy that the absorption energy consists of two parts: the interaction energy (E_{int}) and the deformation energy (E_{def}) that occur in the absorption process. Therefore, the following equations are used to calculate these shares:

$$E_{ads} = E_{int} + E_{def} \quad (2)$$

$$E_{\text{int}} = E_{\text{sheet/AMD}} - E_{\text{sheet in complex}} - E_{\text{AMD in complex}} \quad (3)$$

$$E_{\text{def}} = E_{\text{def}}^{\text{sheet}} + E_{\text{def}}^{\text{AMD}} = \left(E_{\text{sheet in complex}} - E_{\text{pristine sheet}}\right) + \left(E_{\text{AMD in complex}} - E_{\text{isolated AMD}}\right) \quad (4)$$

where $E_{\text{sheet in complex}}$ and $E_{\text{AMD in complex}}$ are energies of AMD molecule and nanosheet in the optimized complexes, respectively.

3 Result and discussion

3.1 The structural analysis

To optimize the structure of pristine single layer boron nitride nanosheets using periodic boundary conditions, we select a 2D unit cell of boron and nitrogen atoms which is $a = 10.0042$ Å and $b = 10.0043$ Å in length containing 32 atoms. We optimized this nanosheet by DFT method with HSEH1PBE functional together with basis set 6-311G (d). After optimization of the pristine nanosheet we substituted Al and Ga with B then P and As with N atom then the optimization process has been repeated for doped nanosheets. The quantitative values of bond lengths are shown in Fig. 1.

The next step was the optimization of AMD/nanosheet complexes. In this step the AMD molecule was placed on the outer surface of each above-mentioned nanosheets with vertical distance of about 2.1 Å. To find out the optimum distances between nanosheet and AMD molecule we used the rigid scan for some cases to estimate the most efficient distance. It should be noted that the level of theory in both optimization and rigid scan was HSEH1PBE/6-311G (d). To better explain the details of the adsorption process, it will be useful to compare Figs. 1 and 2.

The boron nitride nanosheet is composed of several symmetric hexagons that have four different adsorption positions for the adsorption of any molecule onto the outer surface of the nanosheet as shown in Fig. 3: adsorption position on B atom (T_1); adsorption position on N atom (T_2); and adsorption position on B-N bond (T_3); adsorption position at hexagonal center (T_4). The logical approach is to put the AMD molecule in each of these positions and measure the amount of adsorption energy (E_{ads}). It is important to note that the AMD molecule has different heads (Br, Cl, F), and each of these heads must be placed on the desired position on the nanosheet to measure the amount of absorption energy. Our experience shows that negligible differences exist in the amounts of adsorption energies when we place the AMD in any of the possible adsorption sites. As mentioned in [49], when the differences in the adsorption energies are "below the range of chemical interest", placing the gas in different positions on the nanosheets provides identical results. Nevertheless, we put the AMD molecule from N-head onto the desired positions on the BN nanosheet. The test result showed that there is a negligible difference among the

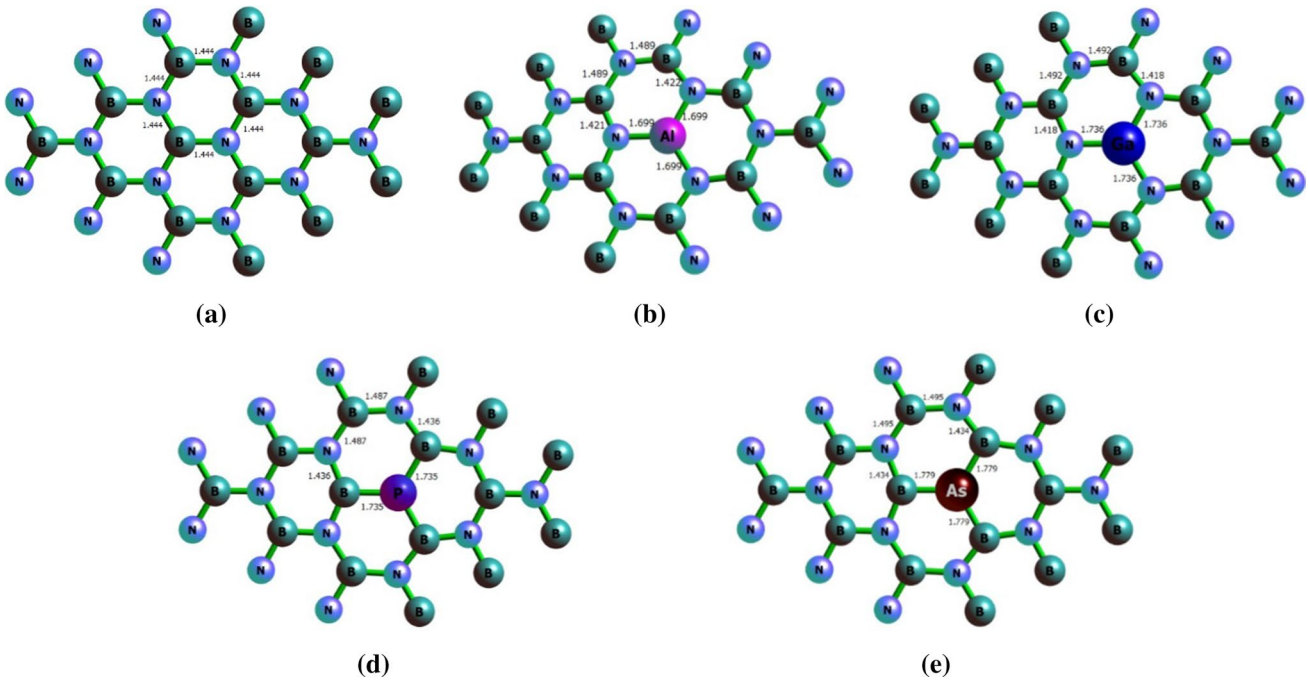

Fig. 1 The values of bond length for **a** BNNS, **b** BNAlNS, **c** BNGaNS, **d** BNPNS, and **e** BNAsNS. The optimization process has been done using HSEH1PBE/6-311G (d) level of theory

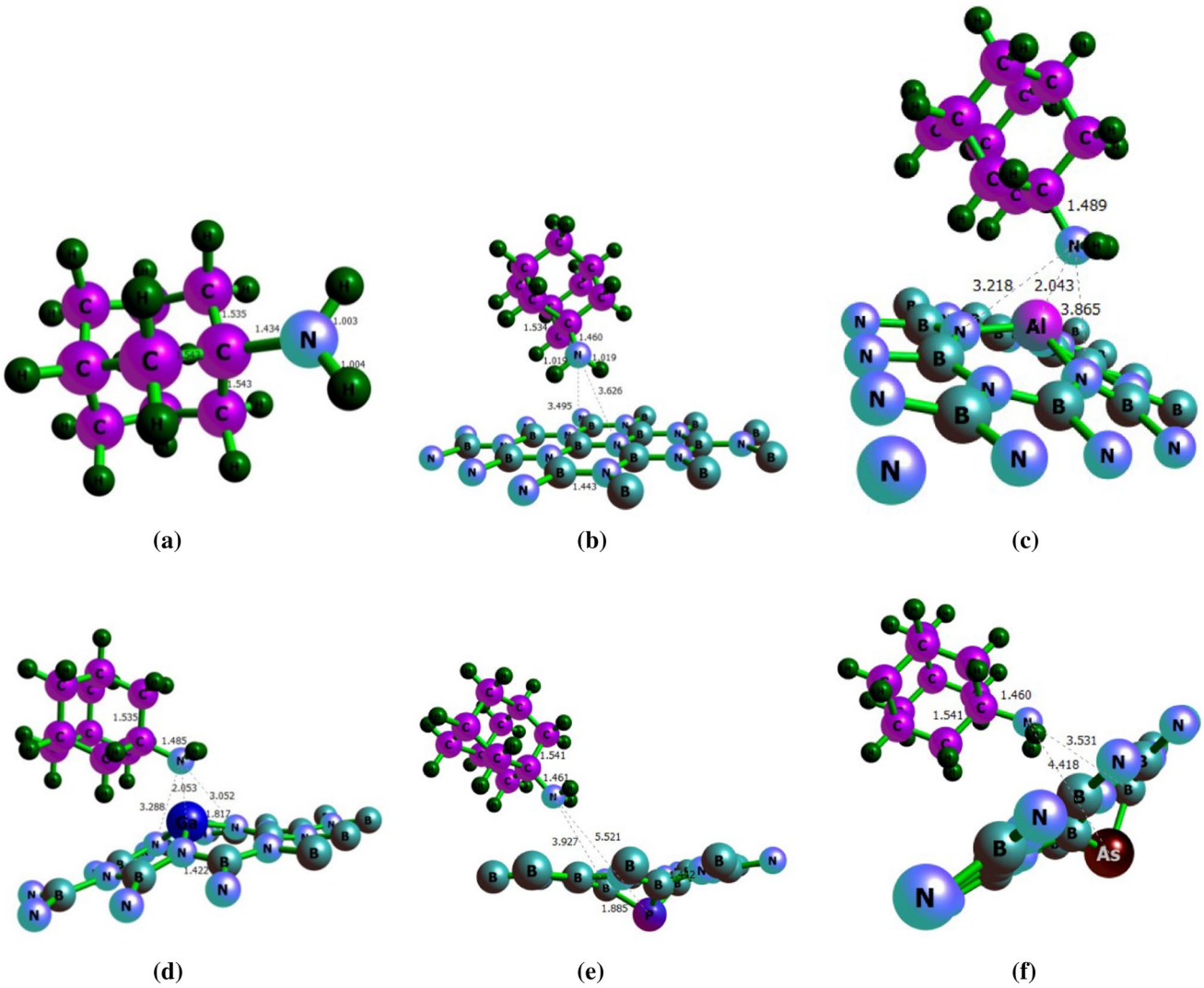

Fig. 2 The most stable form of **a** isolated AMD and the adsorbed AMD molecule onto the outer surface of **a** BNNS, **b** BNAlNS, **c** BNGaNS, **d** BNPNS, and **e** BNAsNS. All clusters have been optimized using the HSEH1PBE functional and 6-311G (d) basis set

adsorption energies; therefore, the boron atom position was the target position on the BN nanosheet.

In the next step, the nanosheet is expanded three times in each directions ($a=25.85$ Å, $b=25.92$ Å) and terminated with hydrogen atom for single point, NBO, and QTAIM studies (Fig. 4). Single point energy calculations using different functional, such as B3LYP-D3, wB97XD, and M062X and 6-311G (d) basis set, were done. The calculated values indicate a strong interactions between nanosheets and AMD molecule. Since the HSEH1PBE functional does not account for the scattering contribution, it is expected that in poor interactions, this functional will not give a good estimate of the amount of energy. For this reason, methods have been developed for effects. One of the most effective, accurate and low computational methods is the experimental method developed by Grimme et al. This method is highly accurate because it has an empirical basis and its parameters are extracted from the spectroscopic experimental data. Various versions of the semi-empirical Grimme method have been presented in recent years [50–52]. In this work we used the latest version of B3LYP-D3known as D3 (BD) (GD3BJ), and wB97XD to consider long range and dispersion effects. The well-known M062X functional are used to better comparison. The results show that the energies obtained from the HSEH1PBE and other functionals are consistent with the accuracy of the calculations. On the other hand, as expected, the B3LYP-D3 method shows more energy values than the others, due to the dispersion contribution consideration. Also by doping the Al, Ga, P, and As elements on the BN nanosheet, significant changes in the results are achieved. Table 1 shows that doping Al, Ga, P, and As increase the absorption energy and enhanced the physical absorption.

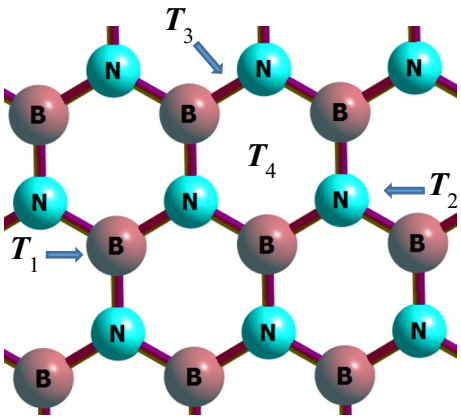

Fig. 3 All possible target positions for the adsorption of any arbitrary molecules onto the surface of BNNS. Top of boron atom (T_1), top of nitrogen atom (T_2), between boron and nitrogen atoms (T_3), and top of the hexagonal ring (T_4)

3.2 Energetics properties

The chemical electron potential (μ) describes the tendency of electrons to escape from a particular species at the ground state. This quantity is equal to the absolute negative electronegativity obtained from the definition provided by Mulliken, as follows:

$$\mu = -xM \tag{5}$$

Parr et al. [53] used the DFT to show that at a constant external potential, the potential energy of an electron is related to the first derivative of energy relative to the number of electrons, as follows:

$$\mu = \left(\frac{\partial E}{\partial N}\right)_{\upsilon(r)} = -\frac{1}{2}(\mathrm{IP} + \mathrm{EA}) \tag{6}$$

where IP and EA are the ionization affinity and electron affinity, respectively [54]. Based on the Koopman's approximation (In the Hartree–Fock theory) and Janak's approximation [55] (in the DFT theory), the ionization and electron affinity potentials are equal to the negative value of the highest occupied molecular orbital (HOMO) energy ($\varepsilon_{\mathrm{HOMO}} = -\mathrm{IP}$) and negative value of the lowest unoccupied molecular orbital (LUMO) ($\varepsilon_{\mathrm{LUMO}} = -\mathrm{EA}$). Therefore, the chemical potential in Janak's approximation is defined as

$$\mu = \left(\frac{\partial E}{\partial N}\right)_{\upsilon(\vec{r})} \cong \frac{(\varepsilon_{\mathrm{LUMO}} + \varepsilon_{\mathrm{HOMO}})}{2} \tag{7}$$

where $\varepsilon_{\mathrm{HOMO}}$ and $\varepsilon_{\mathrm{LUMO}}$ are the energies of the HOMO and the LUMO, respectively. N is the number of electrons, E is the total electronic energy of the system, and $\upsilon(r)$ is the external potential.

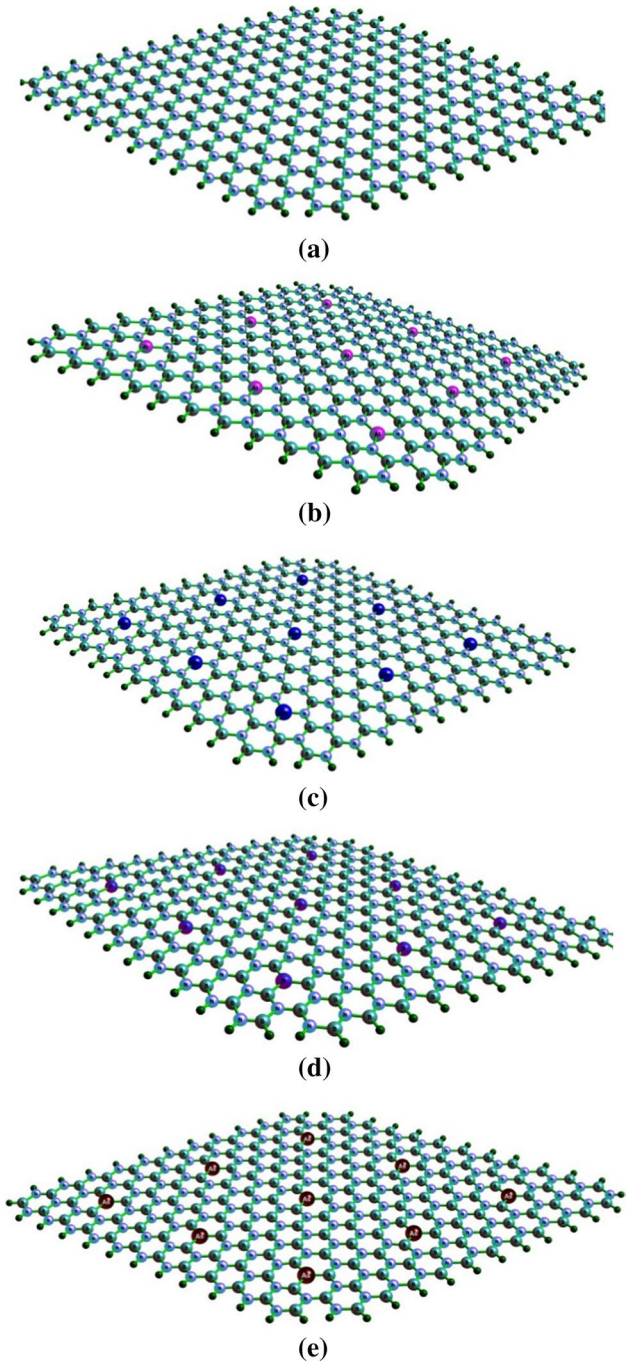

Fig. 4 The 2D **a** boron nitride, **b** Al-doped boron nitride, **c** Ga-doped boron (b), P-doped boron nitride, and **c** As-doped boron nitride nanosheets terminated with hydrogen atoms

Comparison of the variation in electron chemical potentials to that in the number of electrons at a constant external potential is called chemical hardness, which is expressed as

$$\eta = \left(\frac{\partial \mu}{\partial N}\right) = \frac{1}{2}\left(\frac{\partial^2 E}{\partial N^2}\right) \tag{8}$$

Table 1 The interaction energy (E_b) for BNNS, BNAlNS, BNGaNS, BNPNS, and BNAsNS with AMD molecule

System	HSEH1PBE	B3LYP-D3	M06-2X	wB97XD
AMD/BNNS	−0.138	−0.241	−0.160	−0.243
AMD/BNAlNS	−0.783	−0.826	−0.742	−0.831
AMD/BNGaNS	−0.884	−0.867	−0.819	−0.874
AMD/BNPNS	−0.817	−0.802	−0.740	−0.828
AMD/BNAsNS	−0.839	−0.841	−0.755	−0.848

All values are in (eV)

Parr et al. [56] used the electron energy curve as well as the finite difference approximation to express hardness as follows:

$$\eta = \frac{1}{2}(\mathrm{IP} - \mathrm{EA}) \tag{9}$$

Moreover, using Janak and Koopman's approximations, the hardness equation is transformed as follows:

$$\Delta E_{\min} = -\frac{\mu^2}{2\eta} \tag{10}$$

Chemical hardness is the energy gap between the HOMO and the LUMO. Therefore, molecules with high energies are considered as hard molecules, while those with low energies are called soft molecules. Since the softness of a molecule is the opposite of its hardness, the equation for molecule softness is denoted as follows [57]:

$$S = \frac{1}{\eta} \tag{11}$$

Inspired by Maynard's work, Parr et al. [58] introduced electrophilicity as the steady-state energy in which an atom or a molecule at ground state gains by receiving additional electron charges from the environment. The energy changes that lead to such a charge transfer are expressed as follows:

$$\Delta E = \mu \Delta N + \frac{1}{2}\eta(\Delta N)^2 \tag{12}$$

When the system receives electron charges from the environment sufficient to equate its potential to that of the environment, the system is saturated with electrons and can be expressed as follows:

$$\frac{\mathrm{d}\Delta E}{\mathrm{d}\Delta N} = 0 \tag{13}$$

The electron load received from the environment is maximized, and the total energy of the system is eventually minimized. Thus,

$$\Delta N_{\max} = -\frac{\mu}{\eta} \tag{14}$$

$$\Delta E_{\min} = -\frac{\mu^2}{2\eta} \tag{15}$$

Since $\eta > 0$, $\Delta E < 0$ always, and the charge transfer is energetically desirable. Accordingly, Parr et al. proposed the following equation to denote the electrophilicity of electrophilic species.

$$\omega = \frac{\mu^2}{2\eta} \tag{16}$$

In fact, the electrophilicity index is the capacity of a species to accept an arbitrary number of electrons from the environment. In this regard, Nourizadeh and Maihami [59] used electrophilicity in the Diels–Alder reaction and stated that "atoms appear to be arranged in a natural tendency to reach the lowest electrophilicity." This expression is called the minimum electrophilicity principle (MEP).

The values of maximum occupied molecular orbital (HOMO) and lowest occupied atomic orbital (LUMO) and their differences (HLG), chemical potential (μ), chemical hardness (η), and electrophilicity (ω) are reported in Table 2. From the results of this table, it can be seen that by adsorption of AMD molecule onto the outer surface of nanosheets the distance between HOMO and LUMO levels is reduced relative to the pure nanosheet, which shows the greatest decrease in the interaction of the Ga-doped boron nitrogen nanosheet and AMD, which is caused by the molecular energy absorption matched from this position. By doping the elements Al, Ga, P, and As, it is observed that HLG changed. The decrease in HLG for Al and Ga as well as increased for P and As results in an increase in the electrical conductivity and thus an increase/decrease in the metal property of all the nanosheets compared to pure BNNS. It is also noteworthy that the observed changes in HLG after doped Al, Ga, P, and As are mainly due to lower LUMO energy levels. In order to study these changes in the electron structure of the studied cases more closely, the density of state spectra (DOS) will be analyzed in the next section. For a more detailed study of the electron structure changes, the density of state spectra (DOS) are extracted and illustrated in Fig. 5.

From the DOS spectra, it is clear that DOS spectra for all absorption are in agreement with the values of the energy parameters reported in Table 2. The lowest amount of adsorption energy is related to the pristine nanosheet and the highest amount of adsorption energy is for the adsorption of AMD onto the Ga-doped BN nanosheet, the most changes are also observed in the DOS spectrum relative to the Ga-doped nanosheet. In other words, the electron structure changes show a direct relationship with the absorption

Table 2 Values of HOMO energy (ε_H), LUMO energy (ε_L), HOMO and LUMO energy gap (HLG), chemical potential (μ), chemical hardness (η), and electrophilicity (ω)

Systems	ε_H	ε_L	HLG	μ	η	ω
BNNS	−7.022	−1.271	5.751	−4.147	2.876	24.721
BNAlNS	−6.834	−1.186	5.648	−4.010	2.824	22.703
BNGaNS	−6.864	−1.192	5.672	−4.028	2.836	23.007
BNPNS	−6.363	−1.219	5.144	−3.791	2.572	18.478
BNAsNS	−6.239	−1.208	5.031	−3.724	2.515	17.441
AMD/BNNS	−6.297	−1.337	4.960	−3.817	2.480	18.068
AMD/BNAlNS	−5.726	−0.937	4.790	−3.331	2.395	13.288
AMD/BNGaNS	−5.688	−1.030	4.658	−3.359	2.329	13.137
AMD/BNPNS	−5.514	−1.279	4.235	−3.396	2.118	12.213
AMD/BNAsNS	−5.646	−1.337	4.308	−3.491	2.154	13.129

All values are in (eV) and were obtained from completed nanosheet B3LYP-D3/6-311G (d) level of theory

energies. Given the amount of absorption energy, high amount of binding energy, and the structure of DOS spectra obtained in all of these cases, it can be claimed that the adsorption of AMD molecule onto BN, BN (Al), and BN (Ga), BN (P), and BN (As) nanosheets is a strong physical adsorption type.

3.3 NBO analyses

The natural bond orbital (NBO) analysis has been developed based on many-electron molecular wavefunction in terms of localized electron pair bonding units and uses first-order reduced density matrix of the wavefunction [60, 61]. In the NBO approach, a given wavefunction should be transformed into a localized form in which NBOs are considered as local block eigenfunctions of the density matrix. NBO analysis is applicable in both closed-shell and open-shell systems which are calculated from atom-centered basis functions [62]. The mechanism of the energetic analysis of NBO interactions is based on the one-electron effective energy operator (Fock or Kohn–Sham matrix) that arise from the host electronic structure system (ESS). Second-order perturbation theory is one of the highest uses methods for estimating energy effects. For the case of HF or DFT methods, the interactions between NBOs are considered to analyze the wavefunction energetically, with the explanation that the Kohn–Sham matrix elements are implemented in the DFT platform [63–73].

We used the B3LYP-D3/6-311G (d) level of theory to perform the NBO calculations. The concept of bonded orbitals can be used to understand the distribution of electrons in atomic and molecular orbitals. Atomic charges and molecular bonds can be used to obtain these orbitals. In this method, an electron density matrix is used to both define the shapes of the atomic orbitals in the molecular environment and obtain molecular bonds (electron density between atoms). NBO is defined as the following equation for σ bonding between atoms A and B.

$$\sigma_{AB} = C_A h_A + C_B h_B \tag{17}$$

where h_A and h_B are natural hybrids on the A and B atoms. In the covalent limit, $C_A = C_B$, and at the ionic limit, $C_A \gg C_B$ (if the electronegativity of A is greater than B). Each bonding NBO must be paired with a corresponding antibonding NBO.

$$\sigma^*_{AB} = C_A h_A - C_B h_B \tag{18}$$

Binding orbital analysis is used to evaluate the effects of non-stationary effects, such as anomeric effect, rotation barrier, hydrogen bonding, and so on. In NBO analysis, molecular energy is divided into two parts: total energy (for non-stationary enters) and Lewis molecule energy (where super-conjugation does not occur, and the electrons are strongly bound in single bonds and pairs). The occupied NBOs describe the covalent effects in the molecule, while the non-occupied NBOs are used to describe non-covalent effects. The most important non-occupied NBOs are antibond orbitals [60, 72, 73].

Various types of bond order analyses are developed to take into account the bond property such as Mulliken bond order analysis [74], Mayer bond order analysis [75, 76], multi-center bond order analysis [77, 78], Wiberg bond order analysis [79], fuzzy bond order [80, 81] and so on. Due to the different assumptions, caution should be exercised when using the above-mentioned methods and the term "*Caveat emptor*" in this case is a practical example to describe such a situation. Basis set containing diffuse functions as case in point, leads to unreliable result for Mulliken or Mayer analyses [46]. According to the literature [82], the Wiberg bond order, in comparison to the Mayer method, has much less sensitivity to the basis set. The Wiberg bond index (WBI) is the sum of squares of off-diagonal density matrix elements between atoms and is denoted as follows:

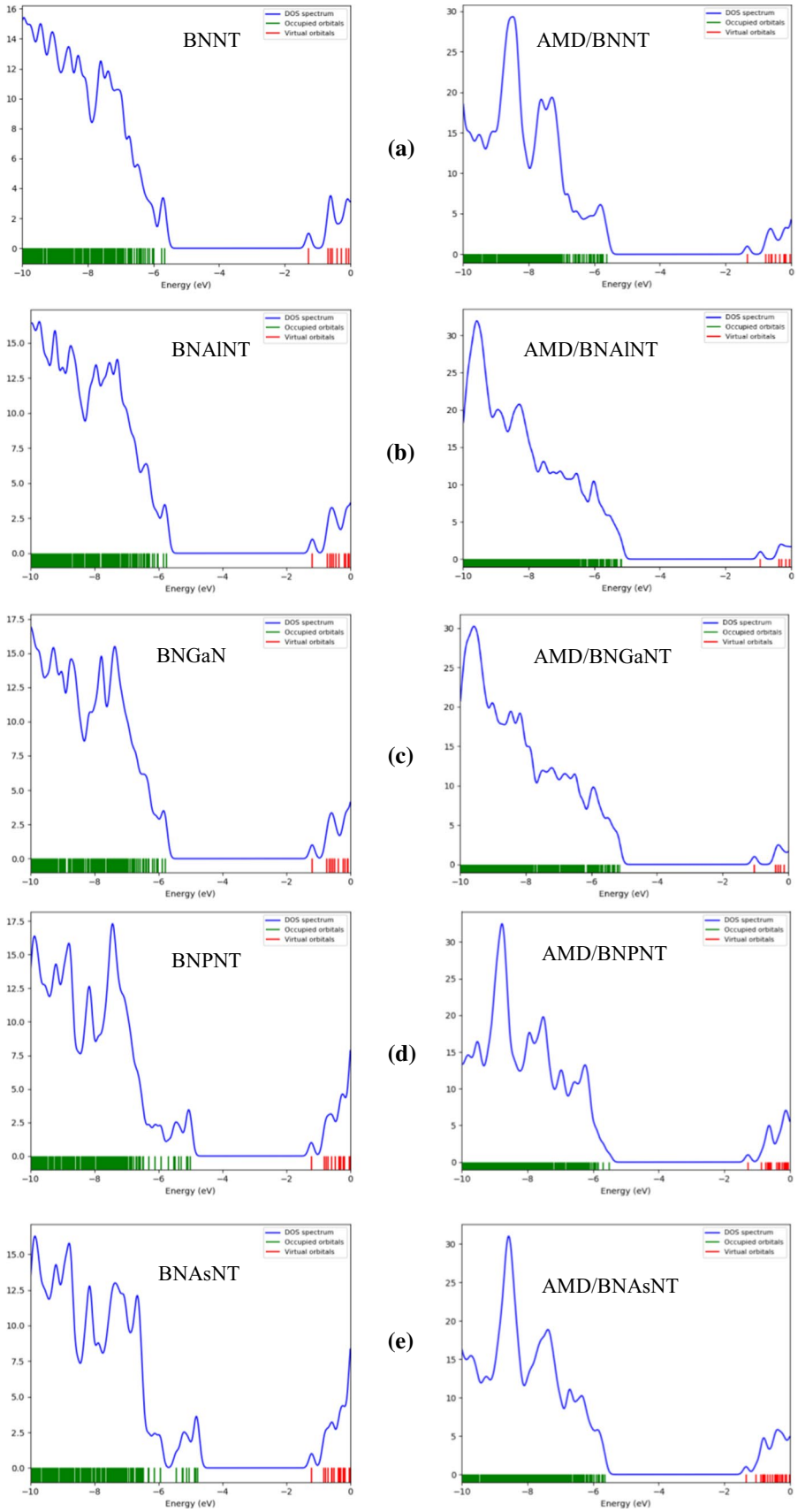

Fig. 5 The density of state (DOS) diagrams for the adsorption of AMD molecule onto the surface of the **a** pristine, **b** Al-doped, **c** Ga-doped, **d** P-doped, and **e** As-doped boron nitride nanosheets. The data were obtained from completed nanosheet and B3LYP-D3/6-311G (d) level of theory. The left side diagrams are isolated nanosheets and the right side diagrams are AMD/nanosheet clusters

$$WBI = \sum_{k} p_{jk}^2 = 2p_{jj} - p_{jj}^2 \tag{19}$$

where P_{jk} represents the density matrix elements (i.e., the contribution of interactions between basis functions j and k) and P_{jj} is the charge density in the atomic orbital. In the WBI, there is no difference between net bonding or antibonding type of elements of the density matrix.

NBO analysis was used to calculate the bond order using the Wiberg method [79] for a more detailed examination of the types of interactions. After studying the adsorption energy of the complexes, we examine the bond length and bond order of the gases and the nanosheets before and after the adsorption. The Wiberg bond orders for these clusters are reported in Table 3. According to this table, that the bond of the halogen atoms in AMD molecules oriented to the N in BNNS, Al in BNAlNS, Ga in BNGaNS, P in BNPNS, and As in BNAsNS are the most significant bonds. The results of the WBI analysis agree with the adsorption energies reported in Table 1. They reveal that these nanosheets show a strong interaction with the gas molecules and can be considered a suitable sensor for such gases.

One of the results of the natural population analysis obtained from NBO calculation is a natural electron configuration which shows the effective valence electron configuration for any atoms in the studied structure. The results of the NBO calculations shed light on the natural electron configuration and partial natural charge, which are useful in the study of the character of the bond between the AMD and the nanosheets. The NBO approach was implemented for all atoms in the pristine and cluster systems to reveal the quantities listed in Table 4. Charge transfer quantity between AMD molecule and nanosheets can also be a criteria to study the interaction of nanosheet and AMD, such that the stronger the interaction the more the charge transfer between AMD and the nanosheet. Table 4 shows that there is a significant charge transfer between two species during adsorption process would be happened.

In addition, by implementing the natural electron configuration the type of the interaction between nanosheets and AMD molecule will be described. From Table 4 it can be obvious that valance configuration of isolated AMD molecule and nanosheets as well as valance configuration of nanosheet/AMD clusters have been increased. Therefore, the interaction of AMD with all nanosheets can be classified as a strong physisorption process.

The second-order perturbation theory is an estimate of donor–acceptor interactions in the NBO basis. NBO analysis expresses the complex quantum–mechanical wavefunction into a more palpable Lewis-dot-like formalism. Lewis-type NBOs are called filled or "*donor*" orbitals (σ) and Non-Lewis-type NBOs are called vacant or "*acceptor*" orbitals (σ^*). For each donor NBO (i) and acceptor NBO (j), the stabilization energy $E(2)$ is calculated as follow [70]:

$$E(2) = \Delta E_{ij}^2 = -q_i \frac{(F_{i,j})^2}{(\varepsilon_j - \varepsilon_i)} \tag{20}$$

where ε_i, ε_j are diagonal elements which show the orbital energies, q_i denotes the donor orbital occupancy ($q=2$ for closed-shell systems and $q=1$ for open-shell systems), and the off-diagonal NBO Fock matrix element is demonstrated by $F(i, j)$, and ΔE_{ij}^2 is the stabilization energy.

The results of electron donor–acceptor electron configuration of pristine BNNS and doped BN (Al), and BN (Ga) nanosheets are reported in Table 6. It is noteworthy that in this table the most important interactions in terms of the electron transfer stability energy are reported. The existence of such interactions with the remarkable stability energies in this table shows that in all cases the doped atom has been incorporated into the nanosheet structure by the chemical interaction and the stability structure has been achieved. In other words, the inserted atom behaves as a doping atom. The data in Table 5 show that the most important interaction for the pristine nanosheet related to electron transfer from the BD (B-x) (x = N, Al, Ga, P, and As) bond as the electron donor to the BD*(N–H) as the receptor. This is in agreement with the results of the absorption energy as well as with the other results which have examined. In the study of the doped complexes, it is observed that in the x- complex, the x electron pair is donor (Lewis base) and the N-bonded electron pair is the group of the electron-acceptor molecule

Table 3 The bond lengths and the nearest intermolecular distances (re (Å)) as well as Wiberg bond index (WBI) between AMD molecule and BNNS, BNAlNS, BNGaNS, BNPNS, and BNAsNS

Systems	N….(x)		N….B		N….N	
	WBI	r(e)	WBI	r(e)	WBI	r(e)
AMD/BNNS	–	–	0.007	3.888	0.001	3.626
AMD/BNAlNS	0.240	2.043	0.002	3.854	0.010	3.006
AMD/BNGaNS	0.296	2.053	0.002	4.125	0.014	3.288
AMD/BNPNS	0.001	5.520	0.044	3.926	0.004	3.213
AMD/BNAsNS	0.001	4.418	0.004	3.530	0.002	3.701

The calculations were performed using PBC-DFT HSEH1PBE/6-311G (d) for bond length and B3LYP-D3/6-311G (d) for WBI (x = Al, Ga, P, and As)

Table 4 Natural electron configurations and natural charges (esu) for the isolated AMD, pristine and Al-, Ga-, P-, and As-doped nanosheets and their complex structures

Systems	Atom	Natural charge	Natural electron configuration
BNNS	B	1.17	[core]2S(0.43)2p(1.38)3p(0.01)3d(0.01)
	N	− 1.17	[core]2S(1.34)2p(4.82)
BNAlNS	B	1.17	[core]2S(0.43)2p(1.38)3p(0.01)3d(0.01)
	N	− 1.17	[core]2S(1.34)2p(4.82)
	Al	2.00	[core]3S(0.39)3p(0.58)3d(0.02)
BNGaNS	B	1.17	[core]2S(0.43)2p(1.38)3p(0.01)3d(0.01)
	N	− 1.17	[core]2S(1.34)2p(4.82)
	Ga	1.80	[core]4S(0.55)4p(0.67)4d(0.01)
BNPNS	B	1.17	[core]2S(0.43)2p(1.38)3p(0.01)3d(0.01)
	N	− 1.17	[core]2S(1.34)2p(4.82)
	P	0.28	[core]3S(1.07)3p(3.64)3d(0.01)
BNAsNS	B	1.17	[core]2S(0.43)2p(1.38)3p(0.01)3d(0.01)
	N	− 1.17	[core]2S(1.34)2p(4.82)
	As	0.35	[core]4S(1.12)4p(3.53)4d(0.01)
AMD/BNNS	B	1.16	[core]2S(0.43)2p(1.39)3p(0.01)3d(0.01)
	N	− 1.17	[core]2S(1.34)2p(4.83)
	C	0.14	[core]2S(0.87)2p(2.98)3p(0.01)3d(0.01)
	N	− 0.89	[core]2S(1.41)2p(4.46)3p(0.01)3d(0.01)
	H	0.37	1S(0.63)
AMD/BNAlNS	B	1.17	[core]2S(0.43)2p(1.40)3p(0.01)3d(0.01)
	N	− 1.18	core]2S(1.41)2p(5.00)3p(0.01)
	Al	2.05	[core]3S(0.39)3p(0.54)3d(0.02)4p(0.01)
	C	0.14	[core]2S(0.88)2p(2.97)3p(0.01)3d(0.01)
	N	− 0.96	[core]2S(1.41)2p(4.54)3p(0.01)
	H	0.43	1S(0.57)
AMD/BNGaNS	B	1.15	[core]2S(0.44)2p(1.37)3p(0.01)3d(0.01)
	N	− 1.15	[core]2S(1.37)2p(4.80)
	Ga	1.83	[core]4S(0.53)4p(0.64)4d(0.01)5p(0.01)
	C	0.14	[core]2S(0.87)2p(2.97)3p(0.01)3d(0.01)
	N	− 0.93	[core]2S(1.41)2p(4.51)3p(0.01)
	H	0.43	1S(0.57)
AMD/BNPNS	B	1.17	[core]2S(0.59)2p(1.64)3p(0.02)3d(0.01)
	N	− 1.17	[core]2S(1.34)2p(4.84)
	P	0.13	[core]3S(1.38)3p(3.48)3d(0.02)4p(0.01)
	C	0.14	[core]2S(1.41)2p(4.45)3p(0.01)3d(0.01)
	N	− 0.88	[core]2S(0.87)2p(2.98)3p(0.01)3d(0.01)
	H	0.38	1S(0.62)
AMD/BNAsNS	B	1.16	[core]2S(0.60)2p(1.65)3p(0.02)3d(0.01)
	N	− 1.16	[core]2S(1.34)2p(4.84)
	As	0.19	[core]4S(1.43)4p(3.37)4d(0.01)5p(0.01)
	C	0.14	[core]2S(0.87)2p(2.98)3p(0.01)3d(0.01)
	N	− 0.89	[core]2S(1.41)2p(4.46)3p(0.01)3d(0.01)
	H	0.37	1S(0.63)
AMD	C	0.14	[core]2S(0.86)2p(2.98)3p(0.01)3d(0.01)
	N	− 0.93	[core]2S(1.29)2p(4.63)3p(0.01)
	H	0.40	1S(0.60)

All values calculated by the HSEH1PBE/6-311G (d) level of theory

Table 5 The donor–acceptor NBO interactions and second order perturbation energies ($E(2)$) for the AMD clusters with BNNS, BNAlNS, BNGaNS, BNPNS, and BNAsNS

Systems	Donor NBO (i)	Acceptor NBO (j)	E2 (kcal/mol)
AMD/BNNS	BD (B-N)	BD*(N–H)	0.09
AMD/BNAlNS	BD (B-Al)	BD*(N–H)	0.61
AMD/BNGaNS	BD (B-Ga)	BD*(N–H)	0.73
AMD/BNPNS	BD (B-P)	BD*(N–H)	0.24
AMD/BNAsNS	BD (B-As)	BD*(N–H)	0.23

All values obtained from completed nanosheets at the HSEH1PBE/6-311G (d) level of theory

(Lewis acid). The highest electron-acceptor stabilization energy in all cases is due to the same interaction, which indicates a strong adsorption of the molecule onto the BN (Ga) nanosheet compared to the others.

3.4 QTAIM analysis

QTAIM is a powerful tool for topology analysis containing the type and structure of bonds and intermolecular interactions. QTAIM method was proposed by Bader et al. [83–88]. According to this theory, the critical point of the electron density, which can be a minimum point, a maximum point, or a saddle point, can fall into one of the following four categories: (1) *Atomic critical point* (ACP), which denotes the geometrical position of an atom or nucleus (other than hydrogen), and geometrically represents a local maximum point of electron density in all three directions of space; (2) *bond critical point* (BCP), which indicates a critical point related to a bond or physical or chemical interaction (in reality, this point represents a saddle point with two directions of maximum electron density and one direction of minimum electron density); (3) *ring critical point* (RCP) [89, 90], which denotes a ring or set of atoms forming a ring (geometrically, it is a saddle point with the minimum electron density in one direction and in the other two directions); and (4) *cage critical point* (CCP), which is observed when multiple rings form a cage (geometrically, this point is a local minimum point in all three directions of space). Poincaré–Hopf relationship should be satisfied to verify if all CPs may have been found as follows [91, 92]:

$$n_{(\mathrm{ACP})} - n_{(\mathrm{BCP})} + n_{(\mathrm{RCP})} - n_{(\mathrm{CCP})} = 1 \tag{21}$$

The eigenvalues of Hessian matrix, λ_1 and λ_2, are negative and $|\lambda_1| < |\lambda_2|$ for the BCP. λ_1 and λ_2 are perpendicular to the bonding path, and λ_3 is a positive value along the bonding path. For the QTAIM analysis, it is necessary to know the electron density $\rho(r)$ and Laplacian electron density $\nabla^2\rho(r)$. The $\rho(r)$ and $\nabla^2\rho(r)$ play an important role in the segmentation and identification of different types of chemical interactions. A BCP with negative values of $\nabla^2\rho(r)$ and large values of $\rho(r)$ (of orders exceeding 10−1 a.u.) is defined as a shared (covalent) intermolecular interaction. Also, when $\nabla^2\rho(r)$ is positive, the interactions can be classified as of the non-substrate close-shell type (which include ionic and van der Waals interactions) [93]. The elliptical bond (ε) [94] and the virial theorem [95] are two other important factors in the classification of bonds. An elliptical bond represents the electron density preferentially accumulated on a plate containing the bond and is defined as follows:

$$\varepsilon = \frac{\lambda_1}{\lambda_2} - 1 \quad \text{where } |\lambda_1| > |\lambda_2| \tag{22}$$

Large values of ε indicate an unstable structure and vice versa. Also, based on the virial theorem, the following relationship exists between the electron kinetic energy density $G(r)$ [96], the electron potential energy density $V(r)$ [97], and $\nabla^2\rho(r)$:

$$\frac{1}{4}\nabla^2\rho(r) = 2G(r) + V(r) \tag{23}$$

The balance between $G(r)$ and $V(r)$ reflects the nature of the interaction, and therefore, the ratio of $G/|V|$ can be used as an appropriate index in link classification. If this ratio is less than 0.5, the nature of the interaction will be purely covalent, and if the ratio is greater than 1, the interaction may be considered as completely non-covalent. Note that for

Table 6 The AIM topological parameters, including electron density ($\rho(r)$), Laplacian of electron density ($\nabla^2\rho(r)$), the kinetic electron density $G(r)$, potential electron density $V(r)$, eigenvalues of Hessian matrix (λ) and bond ellipticity index (ε) at BCPs of the AMD clusters with BNNS, BNAlNS, BNGaNS, BNPNS, and BNAsNS

Systems	Bond	ρ	$\nabla^2 r$	$G(r)$	$V(r)$	$G(r)/V(r)$	λ_1	λ_2	λ_3	ε
AMD/BNNS	N….B	0.0025	0.0084	0.0016	−0.0011	1.4178	−0.0003	−0.0014	0.0101	3.4508
AMD/BNAlNS	N….Al	0.0523	0.2711	0.0684	−0.0690	0.9911	−0.0727	−0.0711	0.4149	0.0229
AMD/BNGaNS	N….Ga	0.0773	0.3000	0.0933	−0.1115	0.8363	−0.0926	−0.0923	0.4850	0.0034
AMD/BNPNS	N….P	0.0036	0.0119	0.0023	−0.0016	1.4457	−0.0022	−0.0016	0.0157	0.3564
AMD/BNAsNS	N….As	0.0046	0.0158	0.0030	−0.0021	1.4255	−0.0034	−0.0020	0.0212	0.6602

All values have been calculated using the B3LYP-D3/6-311G (d) level of theory from NBO analysis

covalent bonds (i.e., $\nabla^2\rho(r)<0$ and $G/|V|<0.5$), the nature of the bond changes from van der Waals interactions to strong covalent interactions, it becomes covalent. It can also play a decisive role in controlling the amount of ionic interaction for close-shell interactions (i.e., $\nabla^2\rho(r)>0$ and $G/|V|>1$), as they become stronger ionically (and weakly electrostatic) by reducing interactions. Therefore, the QTAIM topology analysis together with WBI analysis and adsorption results expose an important trend: by increasing the ionic character of atomic bonds in the nanosheets, the tendencies of the gases to adsorb is also increased.

Considerable results can be obtained from reviewing Table 6. It is observed that in all adsorption sites Laplacian of electron energy density has a positive value, i.e., the bond is non-covalent. In the study of doped systems, we found that for the all clusters the energy density and the energy density of Laplacian are high indicating that there is a strong bond between the nanosheets and the AMD molecule and the elliptical bond is close to 0, which means the interaction is strong. As stated above, the ratio $G/|V|$ more than 1 means non-covalent bonding, in the case of Al- and Ga-doped clusters these amounts are less than 1. In other words, the results of QTAIM analysis also confirm the strong adsorption of the AMD molecule on the BN(Al)NT and BN(Ga)NT (Fig. 6).

The reduced density gradient (RDG) function as well as $\operatorname{sign}\lambda_2(r)\rho(r)$ are used to evaluate the weak interactions. These functions are categorized in the context of non-covalent interaction methods which is powerful way to analyze the types of intermolecular interactions. The RGD is defined as follows [98, 99]:

$$RDGs = \frac{1}{2(3\pi^2)^{\frac{1}{3}}}\frac{\left|\overline{\Delta\rho}(r)\right|}{\overline{\rho(r)}^{\frac{4}{3}}} \tag{24}$$

The strength of the interaction has a positive correlation with electron density $\rho(r)$ and the second largest eigenvalue of the Hessian matrix (λ_2). Thus, the real space function $\operatorname{sign}\lambda_2(r)\rho(r)$ (the products of the signs of λ_2 and ρ) can be defined. The scatter graph of the sign of the $\lambda_2(r)\rho(r)$ function (X-axis) and RDG (Y-axis) reveals the interaction type between gases and nanosheets. The RDG values range from medium to very large around the nuclei and edges of the molecules, whereas weak interactions (zero to medium) are observed around the chemical bonds. Also, for each specific value of RDG (seen as a horizontal line on the graph), the regions of the graph can be classified into three types, namely, $\operatorname{sign}\lambda_2(r)\rho(r)<0$ (strong attraction), $\operatorname{sign}\lambda_2(r)\rho(r)\approx 0$ (weak van der Waals interaction), and $\operatorname{sign}\lambda_2(r)\rho(r)>0$ [strong repulsion (steric effect in ring)] [98, 99].

Using the isosurface RDG = 0.5 as a reference, it can be concluded that after adsorption of the gas onto the outer surfaces of the nanosheets, spots appeared around the region characterized by $\operatorname{sign}\lambda_2(r)\rho(r)\approx 0$. The interaction of gas with BN nanosheets is in the range of strong van der Waals interactions in nature. Significant changes in the overall features of the pristine nanosheets graph (Fig. 7) after the adsorption of gases were observed in the region characterized as $\operatorname{sign}\lambda_2(r)\rho(r)<0$ (i.e., strong attraction), implying that the nanosheet/gas interactions were strong. Hence, this analysis also confirms the results of the single-point energy calculations and NBO analysis, namely that the interactions of AMD with BNNS, BNAlNS, BNGaNS, BNPNS, and BNAsNS were strong.

4 Conclusion

In this study, the interactions between amantadine molecule and pristine, Al-doped, Ga-doped, P-doped, and As-doped boron nitride nanosheets as were investigated using density functional framework. To this end, the structure of the nanosheets and AMD molecule was optimized at the theoretical level of HSEH1PBE/6-311G (d). Right after that B3LYP-D3, M062X, and wB97XD functionals and same basis set were also used to consider the contribution of long range interactions and dispersion effect. QTAIM and NBO analyzes were also implemented to consider the character of intermolecular interactions. The results of all analyses are in agreement and show: (1) Among the different positions studied for pristine boron nitride nanosheet, the T_1 position has the highest absorption energy; (2) investigations in this study show that the Al, Ga, P, and As elements can be substituted by BNNS nanosheet atoms by chemical bonding and, as a binding element, cause dramatic changes in the chemical, electronic and mechanical structure of BNNS nanosheets; (3) Among the doped nanosheets, Ga-doped BNNS has a very high adsorption energy compared to other elements, and is expected to be chemically adsorbed in this case and appears to be a suitable sensor characteristic option. The next category is Al element, where the adsorption energy is higher than the initial state but lower than that of Ga. Generally, we found that the adsorption tendencies of the aforementioned gas molecule have a positive correlation to the nature of the bonds in BN nanosheets. Finally, we conclude that the BNNS, BNAlNS, BNGaNS, BNPNS, and BNAsNS are suitable drug delivery options for the AMD molecule.

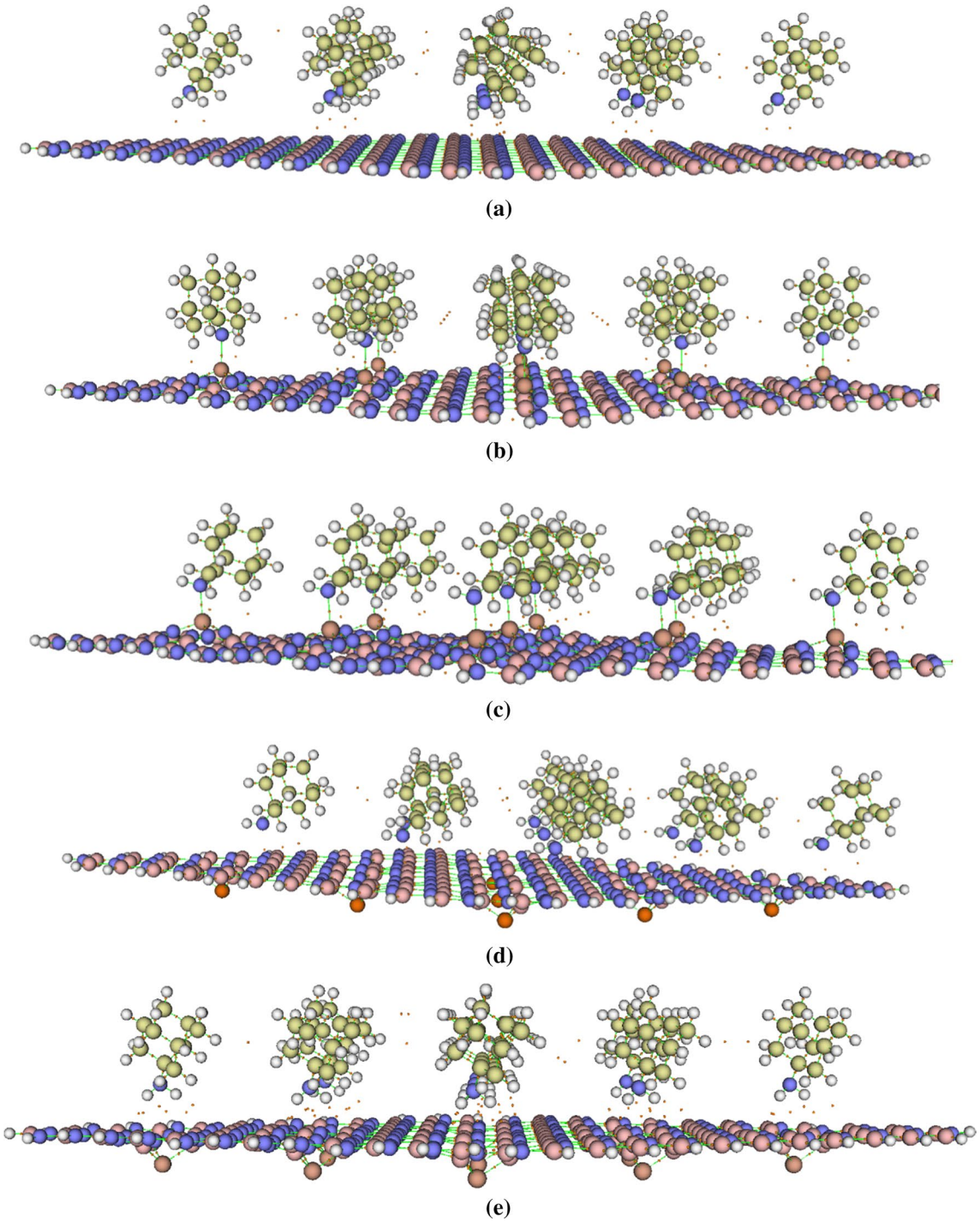

Fig. 6 AIM molecular graphs for **a** AMD/BNNS, **b** AMD/BNAlNS, **c** AMD/BNGaNS, **d** BNPNS, and **e** BNAsNS systems. Orange dots represent the boundary critical points (BCPs)

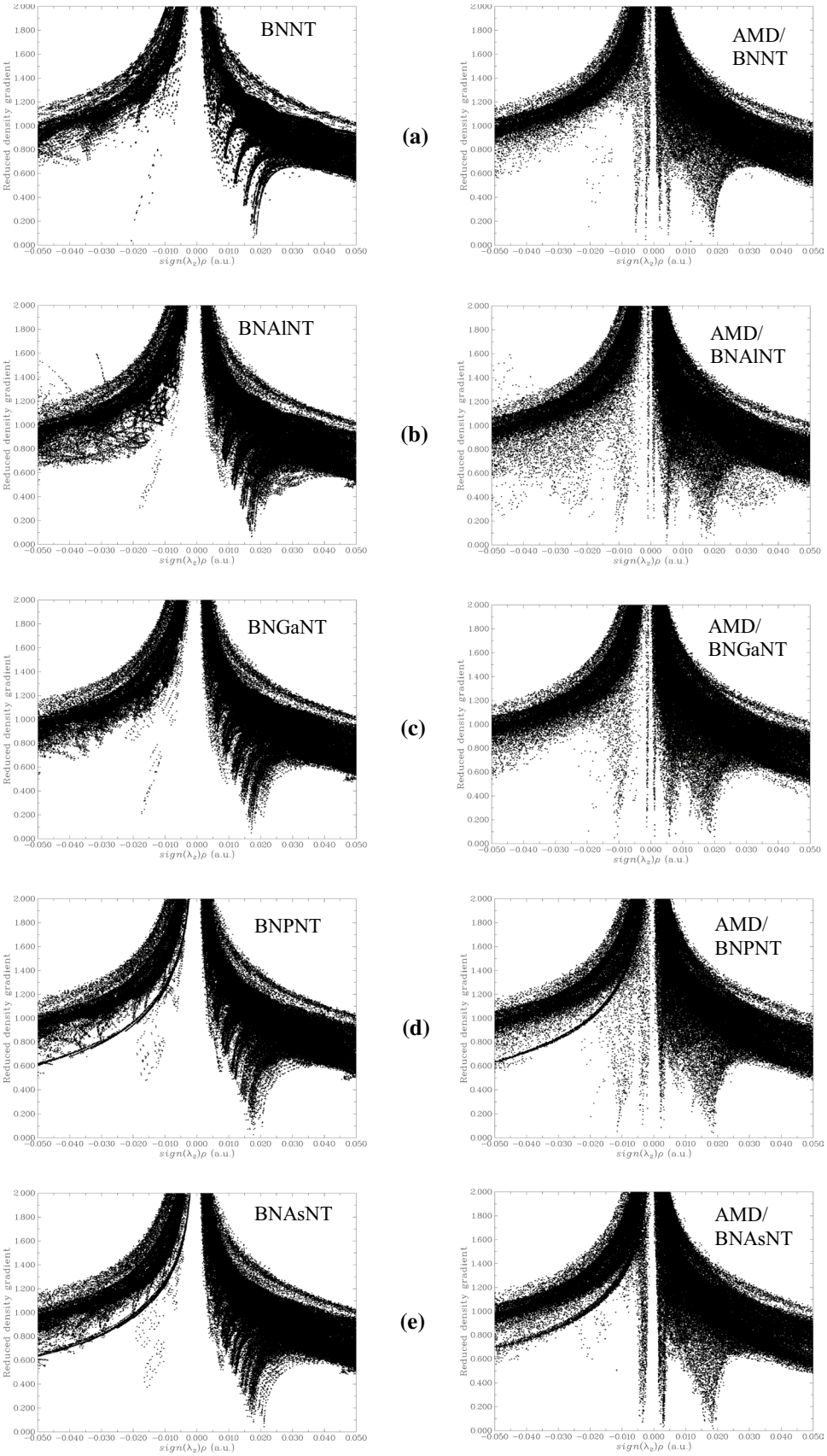

Fig. 7 Plots for the reduced density gradient (RDG) versus sign $(\lambda_2)\rho$(r) values of the **a** pristine, **b** Al-doped, **c** Ga-doped, P-doped, and As-doped boron nitride nanosheets. The data were obtained from completed nanosheet and B3LYP-D3/6-311G (d) level of theory. The left side diagrams are isolated nanosheets and the right side diagrams are AMD/nanosheet clusters

Acknowledgements I would like to thank the Solid-State Theory Group at the Physics Department at the Universita‘ degli Studi di Milano-Italy for providing computational facilities.

Compliance with ethical standards

Conflict of interest The authors declare no conflict of interest.

References

1. Monthioux M, Kuznetsov VL (2006) Who should be given the credit for the discovery of carbon nanotubes? Carbon 44:1621–1623
2. Ghadamgahi M, Ajloo D (2015) Molecular dynamics insight into the urea effect on Tretinoin encapsulation into carbon nanotube. J Braz Chem Soc 26:185–195
3. Chopra NG, Luyken R, Cherrey K, Crespi VH, Cohen ML, Louie SG, Zettl A (1995) Boron nitride nanotubes. Science 269:966–967
4. Rubio A, Corkill JL, Cohen ML (1994) Theory of graphitic boron nitride nanotubes. Phys Rev B 49:5081
5. Golberg D, Bando Y, Tang C, Zhi C (2007) Boron nitride nanotubes. Adv Mater 19:2413–2432
6. Han W-Q, Mickelson W, Cumings J, Zettl A (2002) Transformation of B x C y N z nanotubes to pure BN nanotubes. Appl Phys Lett 81:1110–1112
7. Aldalbahi A, Zhou AF, Feng P (2015) Variations in crystalline structures and electrical properties of single crystalline boron nitride nanosheets. Sci Rep 5:16703
8. Lee KH, Shin H-J, Lee J, Lee I-Y, Kim G-H, Choi J-Y, Kim S-W (2012) Large-scale synthesis of high-quality hexagonal boron nitride nanosheets for large-area graphene electronics. Nano Lett 12:714–718
9. Park J-H, Park JC, Yun SJ, Kim H, Luong DH, Kim SM, Choi SH, Yang W, Kong J, Kim KK (2014) Large-area monolayer hexagonal boron nitride on Pt foil. ACS Nano 8:8520–8528
10. Wu Q, Park J-H, Park S, Jung SJ, Suh H, Park N, Wongwiriyapan W, Lee S, Lee YH, Song YJ (2015) Single crystalline film of hexagonal boron nitride atomic monolayer by controlling nucleation seeds and domains. Sci Rep 5:16159
11. Yu J, Qin L, Hao Y, Kuang S, Bai X, Chong Y-M, Zhang W, Wang E (2010) Vertically aligned boron nitride nanosheets: chemical vapor synthesis, ultraviolet light emission, and superhydrophobicity. ACS Nano 4:414–422
12. Lin Y, Connell JW (2012) Advances in 2D boron nitride nanostructures: nanosheets, nanoribbons, nanomeshes, and hybrids with graphene. Nanoscale 4:6908–6939
13. Li LH, Chen Y (2016) Atomically thin boron nitride: unique properties and applications. Adv Func Mater 26:2594–2608
14. Falin A, Cai Q, Santos EJ, Scullion D, Qian D, Zhang R, Yang Z, Huang S, Watanabe K, Taniguchi T (2017) Mechanical properties of atomically thin boron nitride and the role of interlayer interactions. Nat Commun 8:1–9
15. Guerra V, Wan C, McNally T (2019) Thermal conductivity of 2D nano-structured boron nitride (BN) and its composites with polymers. Prog Mater Sci 100:170–186
16. Li J-L, Yin J-H, Ji T, Feng Y, Liu Y-Y, Zhao H, Li Y-P, Zhu C-C, Yue D, Su B (2019) Microstructure evolution effect on high-temperature thermal conductivity of LDPE/BNNS investigated by in situ SAXS. Mater Lett 234:74–78
17. Yang X, Guo Y, Han Y, Li Y, Ma T, Chen M, Kong J, Zhu J, Gu J (2019) Significant improvement of thermal conductivities for BNNS/PVA composite films via electrospinning followed by hot-pressing technology. Compos B Eng 175:107070
18. Liu L, Ryu S, Tomasik MR, Stolyarova E, Jung N, Hybertsen MS, Steigerwald ML, Brus LE, Flynn GW (2008) Graphene oxidation: thickness-dependent etching and strong chemical doping. Nano Lett 8:1965–1970
19. Li LH, Cervenka J, Watanabe K, Taniguchi T, Chen Y (2014) Strong oxidation resistance of atomically thin boron nitride nanosheets. ACS Nano 8:1457–1462
20. Li LH, Xing T, Chen Y, Jones R (2014) Boron nitride nanosheets for metal protection. Adv Mater Interfaces 1:1300132
21. Liu Z, Gong Y, Zhou W, Ma L, Yu J, Idrobo JC, Jung J, MacDonald AH, Vajtai R, Lou J (2013) Ultrathin high-temperature oxidation-resistant coatings of hexagonal boron nitride. Nat Commun 4:1–8
22. Hu S, Lozada-Hidalgo M, Wang F, Mishchenko A, Schedin F, Nair R, Hill E, Boukhvalov D, Katsnelson M, Dryfe R (2014) Proton transport through one-atom-thick crystals. Nature 516:227–230
23. Fu L, Chen G, Jiang N, Yu J, Lin C-T, Yu A (2016) In situ growth of metal nanoparticles on boron nitride nanosheets as highly efficient catalysts. J Mater Chem A 4:19107–19115
24. Luo W, Wang Y, Hitz E, Lin Y, Yang B, Hu L (2017) Solution processed boron nitride nanosheets: synthesis, assemblies and emerging applications. Adv Func Mater 27:1701450
25. Raza MA, Nadeem A, Ilyas MT (2019) Corrosion study of boron nitride nanosheets deposited on copper metal by electrophoretic deposition. In: TMS 2019 148th annual meeting & exhibition supplemental proceedings, Springer, pp 681–685
26. Omidirad R, Azizi K (2019) DFT study of charge-controlled mechanism of water molecule dissociation on vacancy defected boron nitride nanosheets. J Mol Graph Model 93:107448
27. Esrafili MD, Saeidi N (2018) Carbon-doped boron nitride nanosheet as a promising catalyst for N2O reduction by CO or SO2 molecule: a comparative DFT study. Appl Surf Sci 444:584–589
28. Esrafili MD (2018) NO reduction by CO molecule over Si-doped boron nitride nanosheet: a dispersion-corrected DFT study. Chem Phys Lett 695:131–137
29. Esrafili MD, Mousavian P, Rad FA (2018) Adsorption of formamide over pristine and Al-doped boron nitride nanosheets: a dispersion-corrected DFT study. J Mol Graph Model 82:101–107
30. Moladoust R, Esrafili MD, Hosseinian A, Alkorta I, Vessally E (2019) Adsorption sensitivity of pristine and Al-or Si-doped boron nitride nanoflake to COCl2: a DFT study. Mol Phys 117:626–634
31. Esrafili MD (2018) Epoxidation of ethylene over carbon and silicon-doped boron nitride sheets: A comparative DFT study. Solid State Commun 284:35–39
32. Esrafili MD, Asadollahi S, Heydari S (2019) A DFT study on NO reduction to N2O using Al-and P-doped hexagonal boron nitride nanosheets. J Mol Graph Model 89:41–49
33. Nemati-Kande E, Abbasi M, Mohammadi MD (2020) DFT studies on the interactions of pristine, Al and Ga-doped boron nitride nanosheets with CH3X (X = F, Cl and Br). J Mol Struct 1199:126962
34. Dorn RW, Ryan MJ, Kim T-H, Goh TW, Venkatesh A, Heintz PM, Zhou L, Huang W, Rossini AJ (2020) Identifying the molecular edge termination of exfoliated hexagonal boron nitride nanosheets with solid-state nmr spectroscopy and plane-wave DFT calculations. Chem Mater 32:3109–3121
35. Ai Z, Chang B, Xu C, Huang B, Wu Y, Hao X, Shao Y (2019) Interface engineering in the BNNS@ Ti 3 C 2 intercalation structure for enhanced electrocatalytic hydrogen evolution. New J Chem 43:8613–8619
36. Azamat J, Khataee A, Joo SW (2016) Separation of copper and mercury as heavy metals from aqueous solution using functionalized boron nitride nanosheets: A theoretical study. J Mol Struct 1108:144–149

37. Esrafili MD, Saeidi N (2017) A DFT study on the healing of N-vacancy defects in boron nitride nanosheets and nanotubes by a methylene molecule. Int J Quantum Chem 117:e25450
38. Esrafili MD, Saeidi N, Nematollahi P (2016) The healing of B-or N-vacancy defective BNNTs by using CO molecule: a DFT study. New J Chem 40:8024–8031
39. Li H, Chen Z, Fang X, Tie D (2015) Absorption of NH3 on pristine and defected boron nitride nanosheets: a first principle study. Superlattices Microstruct 88:371–376
40. Lin S, Huang J, Gao X (2015) A Cu (111) supported h-BN nanosheet: a potential low-cost and high-performance catalyst for CO oxidation. Phys Chem Chem Phys 17:22097–22105
41. Davies W, Grunert R, Haff R, McGahen J, Neumayer E, Paulshock M, Watts J, Wood T, Hermann E, Hoffmann C (1964) Antiviral activity of 1-adamantanamine (amantadine). Science 144:862–863
42. Mucke H (2017) Repurposing for Alzheimer's and Parkinson's diseases. In: Dudley J, Berliocchi L (eds) Drug repositioning: approaches and applications for neurotherapeutics. CRC Press, Boca Raton
43. Perdew JP, Burke K, Ernzerhof M (1996) Generalized gradient approximation made simple. Phys Rev Lett 77:3865
44. Hehre WJ, Ditchfield R, Pople JA (1972) Self-consistent molecular orbital methods. XII. Further extensions of Gaussian-type basis sets for use in molecular orbital studies of organic molecules. J Chem Phys 56:2257–2261
45. Frisch M, Trucks G, Schlegel H, Scuseria G, Robb M, Cheeseman J, Scalmani G, Barone V, Petersson G, Nakatsuji H (2016) Gaussian, Inc. Wallingford, CT
46. Lu T, Chen F (2012) Multiwfn: a multifunctional wavefunction analyzer. J Comput Chem 33:580–592
47. Lu T, Chen F (2012) Quantitative analysis of molecular surface based on improved Marching Tetrahedra algorithm. J Mol Graph Model 38:314–323
48. Lu T, Chen Q (2020) A simple method of identifying π orbitals for non-planar systems and a protocol of studying π electronic structure. Theoret Chem Acc 139:25
49. Foresman JB, Frisch A (1996) Exploring chemistry with electronic structure methods: a guide to using Gaussian
50. Grimme S (2006) Semiempirical GGA-type density functional constructed with a long-range dispersion correction. J Comput Chem 27:1787–1799
51. Grimme S, Antony J, Ehrlich S, Krieg H (2010) A consistent and accurate ab initio parametrization of density functional dispersion correction (DFT-D) for the 94 elements H-Pu. J Chem Phys 132:154104
52. Grimme S, Ehrlich S, Goerigk L (2011) Effect of the damping function in dispersion corrected density functional theory. J Comput Chem 32:1456–1465
53. Parr RG, Donnelly RA, Levy M, Palke WE (1978) Electronegativity: the density functional viewpoint. J Chem Phys 68:3801–3807
54. von Szentpály L (1998) Valence states in molecules. 3. Transferable vibrational force constants from homonuclear data. J Phys Chem A 102:10912–10915
55. Janak J (1978) Proof that∂ e∂ n i = ε in density-functional theory. Phys Rev B 18:7165
56. Parr RG (1980) Density functional theory of atoms and molecules. In: Fukui K, Pullman B (eds) Horizons of quantum chemistry. Springer, Berlin, pp 5–15
57. Chattaraj P, Roy D (2007) Perennial review: update 1 of Chem. Rev. 106, 2065 (2006). Chem Rev 107
58. Parr RG, Szentpaly LV, Liu S (1999) Electrophilicity index. J Am Chem Soc 121:1922–1924
59. Noorizadeh S, Maihami H (2006) A theoretical study on the regioselectivity of Diels-Alder reactions using electrophilicity index. J Mol Struct (Thoechem) 763:133–144
60. Weinhold F (2012) Discovering chemistry with natural bond orbitals. Wiley, Hoboken
61. Weinhold F, Landis CR (2005) Valency and bonding: a natural bond orbital donor-acceptor perspective. Cambridge University Press, Cambridge
62. Carpenter J, Weinhold F (1988) Analysis of the geometry of the hydroxymethyl radical by the "different hybrids for different spins" natural bond orbital procedure. J Mol Struct (Thoechem) 169:41–62
63. Foster AJ, Weinhold F (1980) Natural hybrid orbitals. J Am Chem Soc 102:7211–7218
64. Glendening E, Badenhoop J, Reed A, Carpenter J, Bohmann J, Morales C, Landis C, Weinhold F (2013) NBO 6.0. Theoretical Chemistry Institute, University of Wisconsin, Madison
65. Reed AE, Weinhold F (1983) Natural bond orbital analysis of near-Hartree–Fock water dimer. J Chem Phys 78:4066–4073
66. Reed AE, Weinhold F (1985) Natural localized molecular orbitals. J Chem Phys 83:1736–1740
67. Reed AE, Weinstock RB, Weinhold F (1985) Natural population analysis. J Chem Phys 83:735–746
68. Glendening ED, Landis CR, Weinhold F (2012) Natural bond orbital methods. Wiley Interdiscip Rev Comput Mol Sci 2:1–42
69. Glendening ED, Landis CR, Weinhold F (2019) NBO 7.0: new vistas in localized and delocalized chemical bonding theory. J Comput Chem 40:2234–2241
70. Reed AE, Curtiss LA, Weinhold F (1988) Intermolecular interactions from a natural bond orbital, donor–acceptor viewpoint. Chem Rev 88:899–926
71. Weinhold F (2002) Natural bond orbital methods. Encyclopedia of computational chemistry, 3
72. Weinhold F (2012) Natural bond orbital analysis: a critical overview of relationships to alternative bonding perspectives. J Comput Chem 33:2363–2379
73. Weinhold F, Landis C, Glendening E (2016) What is NBO analysis and how is it useful? Int Rev Phys Chem 35:399–440
74. Mulliken RS (1955) Electronic population analysis on LCAO–MO molecular wave functions. I. J Chem Phys 23:1833–1840
75. Mayer I (1983) Charge, bond order and valence in the AB initio SCF theory. Chem Phys Lett 97:270–274
76. Mayer I (2012) Improved definition of bond orders for correlated wave functions. Chem Phys Lett 544:83–86
77. Giambiagi M, de Giambiagi MS, Mundim KC (1990) Definition of a multicenter bond index. Struct Chem 1:423–427
78. Matito E (2016) An electronic aromaticity index for large rings. Phys Chem Chem Phys 18:11839–11846
79. Wiberg KB (1968) Application of the pople-santry-segal CNDO method to the cyclopropylcarbinyl and cyclobutyl cation and to bicyclobutane. Tetrahedron 24:1083–1096
80. Lu T, Chen F (2013) Bond order analysis based on the Laplacian of electron density in fuzzy overlap space. J Phys Chem A 117:3100–3108
81. Mayer I, Salvador P (2004) Overlap populations, bond orders and valences for 'fuzzy'atoms. Chem Phys Lett 383:368–375
82. Sizova OV, Skripnikov LV, Sokolov AY (2008) Symmetry decomposition of quantum chemical bond orders. J Mol Struct (Thoechem) 870:1–9
83. Bader R, Nguyen-Dang TT, Tal Y (1981) A topological theory of molecular structure. Rep Prog Phys 44:893
84. Bader RF (1985) Atoms in molecules. Acc Chem Res 18:9–15
85. Bader RF (1991) A quantum theory of molecular structure and its applications. Chem Rev 91:893–928
86. Bader RF, Matta CF (2013) Atoms in molecules as non-overlapping, bounded, space-filling open quantum systems. Found Chem 15:253–276

87. Biegler-könig FW, Bader RF, Tang TH (1982) Calculation of the average properties of atoms in molecules. II. J Comput Chem 3:317–328
88. Cortés-Guzmán F, Bader RF (2005) Complementarity of QTAIM and MO theory in the study of bonding in donor–acceptor complexes. Coord Chem Rev 249:633–662
89. Howard S, Krygowski T (1997) Benzenoid hydrocarbon aromaticity in terms of charge density descriptors. Can J Chem 75:1174–1181
90. Noorizadeh S, Shakerzadeh E (2010) Shannon entropy as a new measure of aromaticity, Shannon aromaticity. Phys Chem Chem Phys 12:4742–4749
91. Balanarayan P, Gadre SR (2003) Topography of molecular scalar fields. I. Algorithm and Poincaré–Hopf relation. J Chem Phys 119:5037–5043
92. Roy D, Balanarayan P, Gadre SR (2008) An appraisal of Poincaré–Hopf relation and application to topography of molecular electrostatic potentials. J Chem Phys 129:174103
93. Matta CF (2006) Hydrogen–hydrogen bonding: the non-electrostatic limit of closed-shell interaction between two hydro, hydrogen bonding—new insights. Springer, Berlin, pp 337–375
94. Bohórquez HJ, Boyd RJ, Matta CF (2011) Molecular model with quantum mechanical bonding information. J Phys Chem A 115:12991–12997
95. Grabowski SJ (2012) QTAIM characteristics of halogen bond and related interactions. J Phys Chem A 116:1838–1845
96. Tal Y, Bader R (1978) Studies of the energy density functional approach. I. Kinetic energy. Int J Quantum Chem 14:153–168
97. Keith T, Bader R, Aray Y (1996) Structural homeomorphism between the electron density and the virial field. Int J Quantum Chem 57:183–198
98. Contreras-García J, Johnson ER, Keinan S, Chaudret R, Piquemal J-P, Beratan DN, Yang W (2011) NCIPLOT: a program for plotting noncovalent interaction regions. J Chem Theory Comput 7:625–632
99. Johnson ER, Keinan S, Mori-Sánchez P, Contreras-García J, Cohen AJ, Yang W (2010) Revealing noncovalent interactions. J Am Chem Soc 132:6498–6506

Publisher's Note Springer Nature remains neutral with regard to jurisdictional claims in published maps and institutional affiliations.